Ionics (2021) 27:3627–3637
https://doi.org/10.1007/s11581-021-04129-3

ORIGINAL PAPER

Core shell structure $CoMoO_4$@$CuCo_2O_4$ hybrids as advanced electrode materials for high-performance asymmetric supercapacitors

Bairui Tao[1] · Jingli Li[1] · Fengjuan Miao[1] · Yu Zang[2]

Received: 20 May 2021 / Revised: 30 May 2021 / Accepted: 2 June 2021 / Published online: 15 June 2021

Abstract

$CoMoO_4$ microspheres were deposited on nickel (Ni) foam by simple hydrothermal method, and $CuCo_2O_4$ nanowires were uniformly grown on $CoMoO_4$ microspheres, then $CoMoO_4$@$CuCo_2O_4$ core shell structure composite material was successfully synthesized. The electrochemical test of $CoMoO_4$@$CuCo_2O_4$ electrode was completed by cyclic voltammetry (CV), electrochemical impedance spectroscopy (EIS), and galvanostatic charge–discharge (GCD). These experiment results exhibit that $CoMoO_4$@$CuCo_2O_4$ electrode has excellent capacitance characteristic, including a remarkable specific capacitance of 2639 F g^{-1} at 1 A g^{-1} and an outstanding cycle life with a captaincy retention of 91.6% after 2000 cycles at 30 A g^{-1}. Furthermore, an asymmetric supercapacitor (ASC) based on $CoMoO_4$@$CuCo_2O_4$//activated carbon (AC) exhibited a high energy density of 51.2 W h kg^{-1} at 800.3 W kg^{-1}. These performances strongly demonstrate that the $CoMoO_4$@$CuCo_2O_4$ electrode synthesized by simple methods is an excellent electrode material in the application of supercapacitors (SCs).

Keywords CoMoO4@CuCo2O4 · Core shell structure · Supercapacitors

Introduction

With the rapid development of electronic industry and a large number of applications of portable electronic devices, the development of efficient electrochemical energy storage devices has become the focus of attention [1]. Supercapacitors (SCs) have preferable performance than traditional capacitor and battery in energy storage, including charge–discharge efficiency, high-level energy density, and excellent cycle stability [2]. Therefore, it is of great significance to design and develop electrode materials with high energy density and cycle stability through a simple method [3].

In recent years, transition metal oxides such as Co_3O_4, CuO, and MnO_2 have attracted extensive attention in virtue of their electrochemical activity and cycle stability [4–6]. In the research process, bimetallic oxides such as $NiCo_2O_4$, $FeCo_2O_4$, and $NiMoO_4$ increase the specific surface area and have stronger redox activity and structural stability which show better energy storage performance [7–9]. It is noteworthy that due to the synergistic effect of cobalt and molybdenum atoms, bimetallic oxide $CoMoO_4$ has excellent electrochemical activity and electron/ion transfer rate, which is superior than single metal oxide Co_3O_4 [10]. In particular, the ternary metal oxide $CuCo_2O_4$ has higher redox activity and specific capacitance in alkaline electrolyte, so it has distinguished electrochemical characteristics [11]. The Faraday redox reaction can be further improved by doping and composite electrode surface active materials, so that its performance is preferable than other kinds of single component electrode, which can develop the application potential of SCs.

With the research of SCs, the performance of multi-component heterostructure electrode is superior to those single component electrodes, especially multi-component composite metal oxide. Feng et al. reported that $Ni(OH)_2$/$NiMoO_4$ nanoplate arrays were synthesized by hydrothermal method and the specific capacitance is 1547.3 F g^{-1} at 1

Jingli Li and Bairui Tao are co-first authors

✉ Bairui Tao
tbr_sir@163.com

✉ Fengjuan Miao
miaofengjuan@163.com

[1] College of Communications and Electronics Engineering, Qiqihar University, Heilongjiang 161006, China

[2] College of Materials Science and Engineering, Qiqihar University, Wenhua Street 42, Qiqihar, China

A g^{-1}, which retained 88.1% capacitance after 1000 cycles [12]. Wu et al. reported that $NiCo_2O_4/CoMoO_4$ hierarchical nanosheets electrode achieved an electrochemical performance that its capacitance reached 1730 F g^{-1} at 1 A g^{-1} and it also maintained 76.2% capacitance after 1000 cycles [13]. Nti et al. synthesized $NiMoO_4/CoMoO_4$ nanorods which enabled a high specific capacitance of 1445 F g^{-1} at a current density of 1 A g^{-1} and preserved 78.8% of its initial capacitance after 3000 cycles [14]. Experimental results show that the development of composite metal oxides is a new method to prepare high-performance SCs, which can improve the activity and structural stability of electrodes.

Herein, we propose for the first time to synthesize the $CoMoO_4@CuCo_2O_4$ urchin-like composites on Ni foam by simple methods. The $CoMoO_4@CuCo_2O_4$ electrode exhibits an excellent specific capacitance of 2639 F g^{-1} at a current density of 1 A g^{-1} and an outstanding cycle life with a captaincy retention of 91.6% after 2000 cycles at 30 A g^{-1}. In addition, the $CoMoO_4@CuCo_2O_4$//active carbon (AC) asymmetric supercapacitor (ACS) device exhibits a high energy density of 51.2 W h kg^{-1} at 800.3 W kg^{-1}. As a result of the special core shell structure, the $CoMoO_4@CuCo_2O_4$ electrode reveals excellent specific capacitance and structural stability, which is a promising electrode material with high performance for energy storage and supply devices.

Experimental section

Material synthesis

All the chemical reagents in the experiment were purchased from Tianjin Comeo Chemical Reagent Co., Ltd. The aqueous solution was prepared with deionized water. Cobalt nitrate hexahydrate ($Co(NO_3)_2{\cdot}6H_2O$), sodium molybdate dihydrate ($Na_2MoO_4{\cdot}2H_2O$), copper chloride dihydrate ($CuCl_2{\cdot}2H_2O$), ammonium fluoride (NH_4F), and urea ($CO(NH_2)_2$) reagents are analytically pure and can be used directly without purification. The Ni foam (thickness 1.5 mm, pore density 100 PPI) was obtained from Guang Sheng Jia New Materials Co., Ltd., China. The process of preparing the solution was completed at room temperature.

Synthesis of $CoMoO_4$ microspheres on Ni foam

Ni foam (1 cm × 1 cm × 0.15 cm) was immersed in deionized water, hydrochloric acid, deionized water, anhydrous ethanol, and deionized water in 5 min. The cleaning process was carried out in an ultrasonic machine for the purpose of removing oxide and impurities on the surface of Ni foam. In the typical synthesis, 0.136 g $Co(NO_3)_2{\cdot}6H_2O$ and 0.087 g $Na_2MoO_4{\cdot}2H_2O$ were dissolved in 40 mL deionized water, and the mixture was fully dissolved in an ultrasonic machine. The mixed solution was transferred to the 50-mL Teflon-lined stainless steel autoclave. The pretreated Ni foam was immersed in the reaction solution and maintained at 10 h at 180 °C to promote the growth of $CoMoO_4$ microspheres and then cooled to room temperature. Then Ni foam was cleaned with deionized water and dried for 12 h at 60 °C. The average mass of $CoMoO_4$ loaded on Ni foam was about 0.90 mg cm^{-2}.

Synthesis of $CoMoO_4@CuCo_2O_4$ urchin-like composites on Ni foam

In the typical synthesis, 0.291 g $Co(NO_3)_2{\cdot}6H_2O$, 0.085 g $CuCl_2{\cdot}2H_2O$, 0.18 g urea, and 0.037 g NH_4F were dissolved in 35 mL deionized water, the mixed solution was transferred into the Teflon-lined stainless steel autoclave, Ni foam was immersed in the surface of the deposited microsphere in the reaction solution, maintained for 5 h at 120 °C, and then cooled to room temperature. Then Ni foam was cleaned with deionized water and calcined for 2 h at 400 °C in air. Finally, surface deposition obtained the $CoMoO_4@CuCo_2O_4$ composites on Ni foam sample. The average mass of $CoMoO_4@CuCo_2O_4$ composites loaded on Ni foam was about 1.50 mg cm^{-2}.

Material characterization

The crystal structures were characterized by X-ray diffraction (XRD, D8-Discovery Bruker, 40 kV, 40 mA, Cu Kα, $\lambda = 1.5406$ Å) for 2θ between 10 and 85°. The morphology of the synthesized samples was further observed by scanning electron microscope (SEM, JEOL-7500F) and transmission electron microscopy (TEM, HITACHI H-7650). The chemical bond properties of the synthesized samples were studied by X-ray photoelectron spectroscopy (XPS, ESCALAB250).

Electrochemical measurements

The electrochemical tests were carried out in 1 M KOH solution and completed by electrochemical workstation. In the electrochemical test of the three-electrode system, the $CoMoO_4@CuCo_2O_4$ electrode was selected as the working electrode, the counter electrode as the platinum electrode, and the reference electrode as the saturated calomel electrode. In the electrochemical test of the two-electrode system, the $CoMoO_4@CuCo_2O_4$ electrode was selected as the positive electrode and active carbon (AC) on Ni foam as the negative electrode. Cyclic voltammetry (CV) and electrochemical impedance spectroscopy (EIS) tests were carried out at Shanghai Chenhua 760E electrochemical workstation. The potential window of − 0.2 ~ 0.6 V was selected for CV test, and the scanning rate was 5 ~ 100 mV s^{-1}. EIS test was performed at a frequency range of 0.01 to 100 kHz with

an AC voltage of 5 mV. In the electrochemical workstation (Zennium, Zahner, Germany), galvanostatic charge–discharge (GCD) test was carried out, and the potential window of 0 ~ 0.45 V was chosen, and different current densities were selected to complete the test. The specific capacitance is calculated according to the discharge curve in the GCD and the following formula:

$$C_s = I\Delta t/m\Delta V \tag{1}$$

where C_s (F g^{-1}) is the specific capacitance, I (A) is the current in the discharge process, Δt (s) is the discharge time, m (g) is the mass of the active substance, and ΔV (V) is the discharge potential window.

According to the specific capacitance, the energy density and power density of supercapacitor can be calculated by the following formula:

$$E = C_s \times \Delta V^2/2 \tag{2}$$

$$P = E/t \tag{3}$$

where E (W h kg^{-1}) is the energy density and P (W kg^{-1}) is the power density of the supercapacitor.

Results and discussion

The construction of the $CoMoO_4$@$CuCo_2O_4$ core shell composites is shown in Fig. 1; the composite material is synthesized without adding adhesive, and the active substance is deposited stably on Ni foam. There are two main steps: a simple hydrothermal deposition process is used to synthesize the $CoMoO_4$ microspheres on the surface of Ni foam, then the $CuCo_2O_4$ nanowires were densely grown on the surface of $CoMoO_4$ microspheres by hydrothermal and annealing methods. The $CoMoO_4$ microspheres are relatively uniform in size and close to each other, which provides a stable support for the growth of the $CuCo_2O_4$ nanowires. Next, the $CuCo_2O_4$ nanowires were grown on the surface of the $CoMoO_4$ microspheres by hydrothermal and annealing methods. Finally, the $CoMoO_4$@$CuCo_2O_4$ core shell composites was synthesized on the surface of Ni foam. The $CuCo_2O_4$ nanowires were grown on the surface of the $CoMoO_4$ microspheres and spread out to the periphery, which promotes the $CoMoO_4$ microspheres to increase the specific surface area and the spacing between each other, resulting in the electrolyte can fully contact with the hybrid substances, and the capacitance performance is significantly improved.

Figure 2a and b shows different magnifications of the SEM image of the $CoMoO_4$ microspheres synthesized on Ni foam. Figure 2b shows that the $CoMoO_4$ microspheres are composed of a certain amount of uniform nanorods, the $CoMoO_4$ microspheres consist of numerous homogeneous nanorods, and nanorods in different directions have grown together and formed different sizes of microspheres on the surface of Ni foam. According to Fig. 2b, the average diameter of the $CoMoO_4$ microspheres is about 3.5 μm. Smaller nanorods were uniformly deposited on the surface of Ni foam, and the surface was no longer smooth, which provided better supporting sites for the $CoMoO_4$ microspheres. As a result, the $CoMoO_4$ microspheres could attach to Ni foam more stably, and it was difficult to fall off from Ni foam in the reaction process. In the following experiments, more $CuCo_2O_4$ nanowires can be firmly deposited on the surface of the $CoMoO_4$ microspheres, thus improving the electrochemical activity and cycling stability of the electrode. Figure 2c and d shows different magnifications of the SEM images of $CuCo_2O_4$ nanowires obtained by hydrothermal method and annealing method. As shown in Fig. 2d, the $CuCo_2O_4$ nanowires grew on the surface of Ni foam with a small amount of nanosheets, and the average diameter of $CuCo_2O_4$ nanowires is 180 nm. The $CuCo_2O_4$ nanowires can improve the electron transfer rate, which make more active

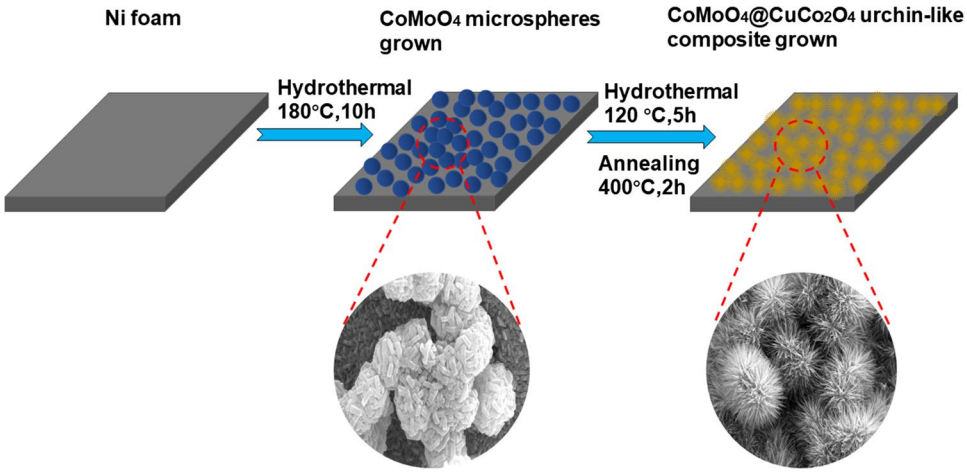

Fig. 1 A schematic diagram of chemical deposition of the $CoMoO_4$@$CuCo_2O_4$ electrode on Ni foam

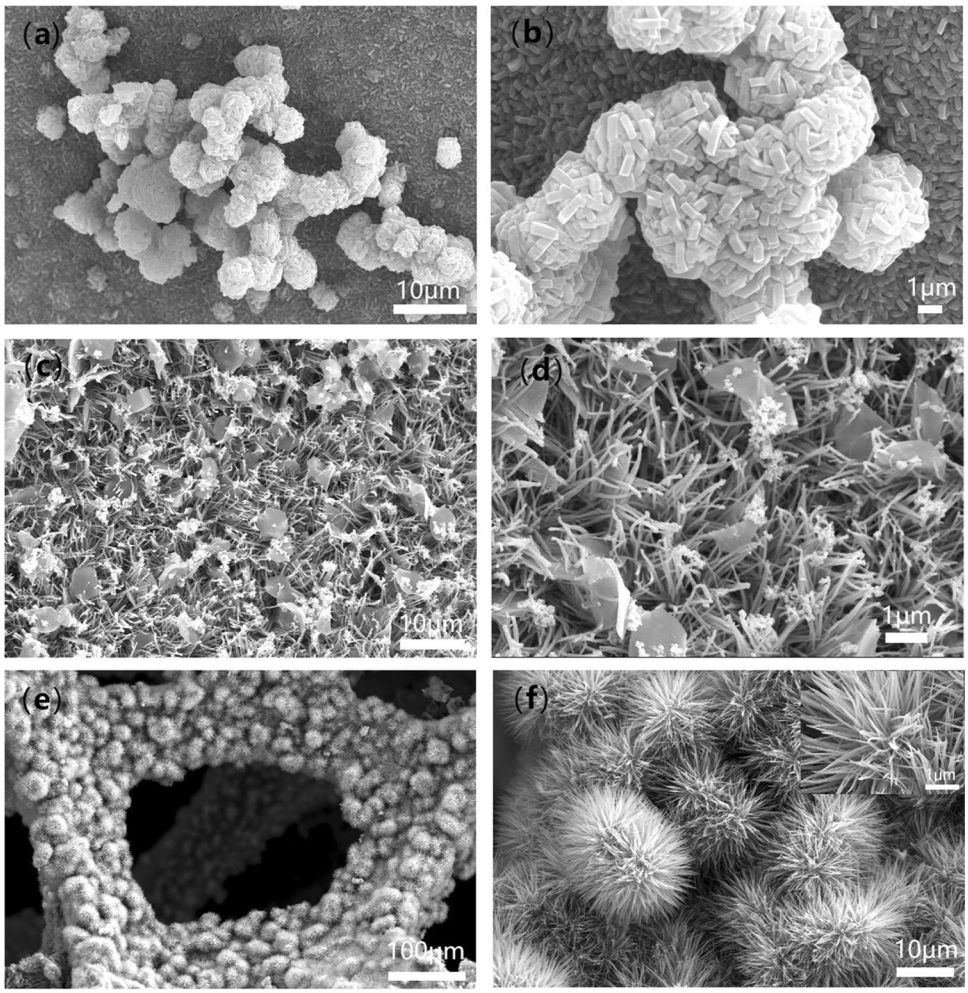

Fig. 2 **a**, **b** SEM image of $CoMoO_4$ microspheres on Ni foam; **c**, **d** SEM image of $CuCo_2O_4$ nanowires on Ni foam; **e**, **f** SEM image of $CoMoO_4$@$CuCo_2O_4$ urchin-like hybrid particles on Ni foam

substances participate in the electrochemical reaction and improve the utilization rate of electrolyte. Figure 2e shows the $CoMoO_4$@$CuCo_2O_4$ with urchin-like uniform distribution on the surface of Ni foam with an average diameter of about 6 μm. The $CoMoO_4$@$CuCo_2O_4$ composite materials are densely distributed on Ni foam, which greatly improves the specific surface area of the electrode. The growth of $CuCo_2O_4$ nanowires reduces the diffusion distance of ions in the electrode. The high-resolution SEM is shown in Fig. 2f and the surface of the structure is arranged with accounts of ordered nanorod arrays, which point toward the center of $CoMoO_4$ microspheres and grows in different directions. As a result of $CoMoO_4$ and $CuCo_2O_4$ having an excellent synergistic effect, the $CoMoO_4$ microspheres have extraordinary electrical conductivity. The $CoCo_2O_4$ nanowires are generated on the $CoMoO_4$ microspheres, which can improve the specific surface area of the electrode and make the active substances in adjacent parts of the composite material participate in the electrochemical reaction, consequently making the electrode exhibit outstanding capacitance performance. Therefore, the urchin-like structure can greatly improve the stability of the structure, thus increasing the contact area between the electrode and electrolyte, which leads to greatly improving the electrochemical activity and conductivity of the electrode.

TEM was used to analyze the internal microstructure of the synthesized active materials. The TEM images of $CoMoO_4$@$CuCo_2O_4$ (core) are shown in Fig. 3a and b. The kernel structure of $CoMoO_4$@$CuCo_2O_4$ is revealed in Fig. 3a and b, which can be clearly observed by transmission electron microscopy that the whole nuclear part presents a uniform distribution state. The color of the core part is darker than that of the edge part, which fully proves that the core is the structure of microspheres, which is consistent with the image results of SEM. The core is made up of the $CoMoO_4$ microspheres, which provide a stable support for the composite electrode to improve its electrochemical activity. The TEM images of the $CuCo_2O_4$ nanowires are exhibited in Fig. 3c and d. The $CuCo_2O_4$ nanowires with uniform size are shown in Fig. 3c and d; they are staggered and distributed to different spatial locations attached to the surface of the $CoMoO_4$ microspheres, making the $CoMoO_4$@$CuCo_2O_4$

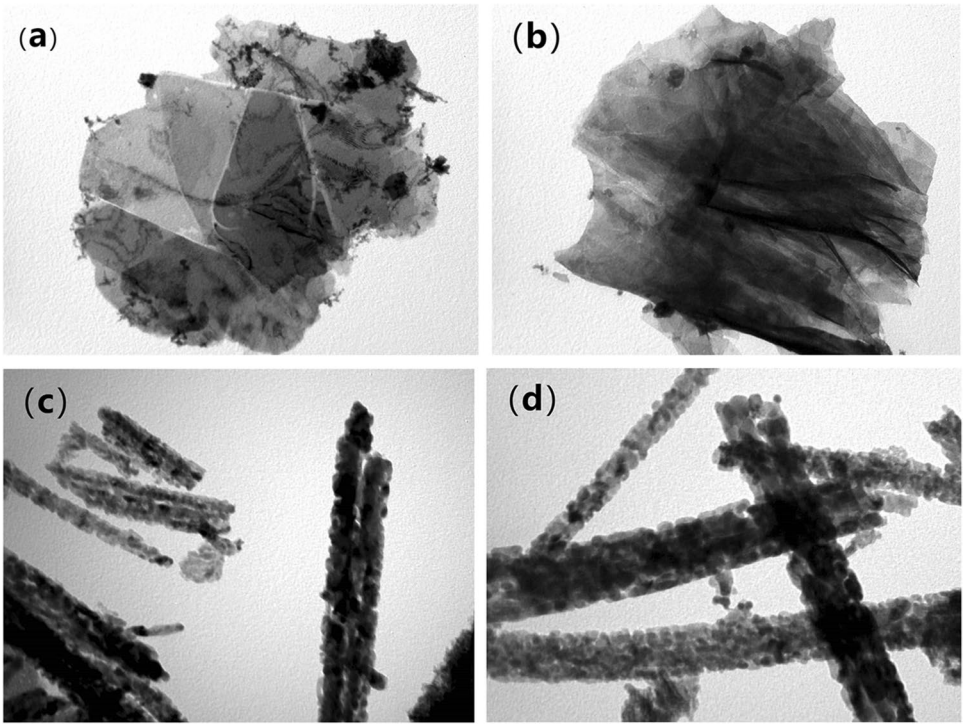

Fig. 3 **a**, **b** TEM image of $CoMoO_4$@$CuCo_2O_4$ (core); **c**, **d** TEM image of $CuCo_2O_4$ nanowires

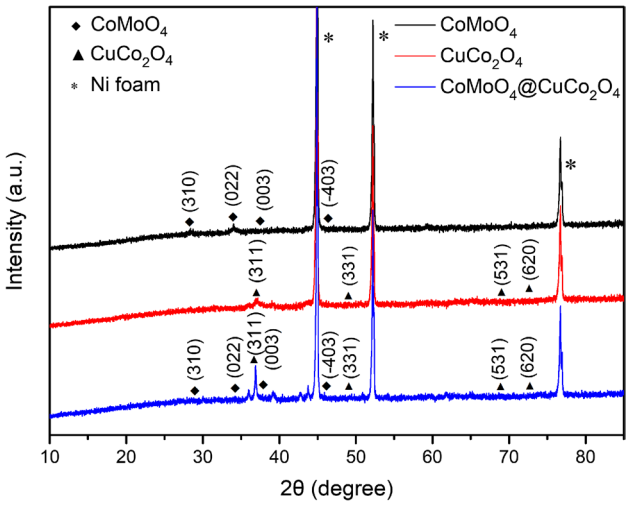

Fig. 4 XRD patterns of $CoMoO_4$, $CuCo_2O_4$, and $CoMoO_4$@$CuCo_2O_4$ grown on Ni foam

composites fully exposed to the electrolyte solution, thus greatly reducing the ion transfer distance. The deposition of the $CuCo_2O_4$ nanowires can improve the utilization rate of active substances and increase the electrical conductivity of the electrode, which is conducive to the full participation of more active substances in the electrochemical reaction.

The phase structure of the synthesized samples is confirmed by XRD analysis. Figure 4 shows the XRD pattern of the $CoMoO_4$ microspheres, $CuCo_2O_4$ nanowires, and $CoMoO_4$@$CuCo_2O_4$ urchin-like hybrid particle arrays on Ni foam. As shown in Fig. 4, there are three different diffraction peaks (111), (200), and (220) at $2\theta = 44.8$, 52.3, and 76.1° (Ni—JCPDS Card No. 01–089-7128) in the three curves, the Ni foam as the substrate accounted for the largest proportion, and these three diffraction peaks were significantly higher than the other diffraction peaks. The black curve shows that the diffraction peaks marked by a diamond point to (310), (022), (003), and (−403) planes of $CoMoO_4$ cubic phase (JCPDS No. 21–0868), and the red curve shows the positions of diffraction peaks at $2\theta = 36.6$, 48.8, 68.2, and 73.6° conform to the (311), (331), (531), and (620) planes of $CuCo_2O_4$ phase (JCPDS Card No. 78–2177). The diffraction peaks of $CoMoO_4$@$CuCo_2O_4$ XRD curve correspond to those of $CoMoO_4$ and $CuCo_2O_4$ respectively, which proves that the $CoMoO_4$ microspheres and $CuCo_2O_4$ nanowires are successfully deposited on Ni foam.

Through XPS analysis of the sample surface, the surface elemental composition and chemical valence state of the $CoMoO_4$@$CuCo_2O_4$ electrode can be comprehensively obtained and Fig. 5 shows the corresponding test curve. The existence of C, Ni, Co, Cu, Mo, and O elements is confirmed by the full spectrum in Fig. 5a. The carbon element is contained in the spectrum because the C 1 s with binding energy of 284.6 eV is used as the reference for calibrating all spectra, and CO_2 in the air is adsorbed on the surface of the sample. In addition, Ni foam is used as the substrate of the electrode, and some of the surface is not completely covered by the composite material; therefore, the

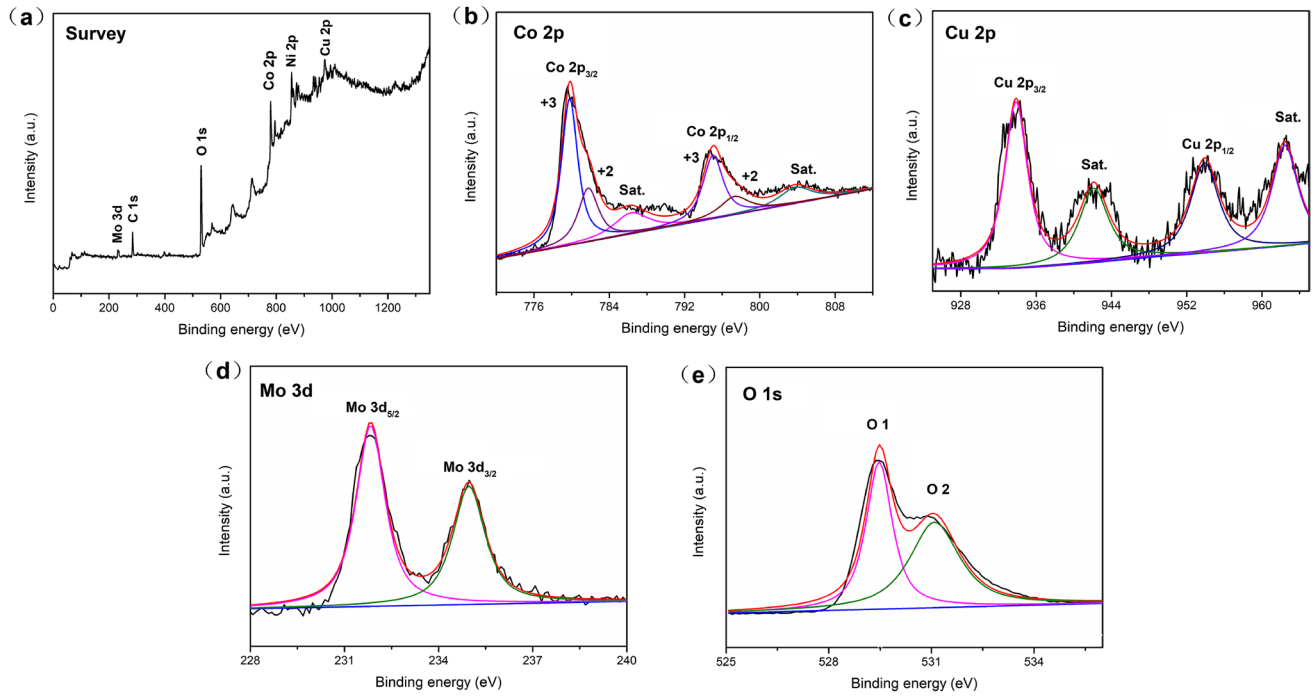

Fig. 5 XPS spectra of $CoMoO_4$@$CuCo_2O_4$ composites, **a** survey scan, **b** Co 2p, **c** Cu 2p, **d** Mo 3d, and **e** O 1 s of the sample

Ni element is observed in the spectrum. The high-resolution XPS spectrum of Co 2p is shown in Fig. 5b. The presence of Co $2p_{3/2}$ and Co $2p_{1/2}$ results in two distinct peaks at 780.1 and 795.5 eV, and the energy gap between the two main peaks is 15.4 eV [15]. Their satellite peaks (labeled as "Sat.") are located at 788.0 and 802.9 eV, which further proves the spinel $CuCo_2O_4$ phase on the sample surface [16]. In addition, the two fitting peaks of 780.6 and 796.6 eV are attributed to Co^{3+}, and the other two fitting peaks of 782.8 and 798.3 eV are attributed to Co^{2+} [17]. Figure 5c shows the high-resolution XPS spectrum of Cu 2p with two distinct peaks at 932.7 and 952.6 eV, which are attributed to Cu $2p_{3/2}$ and Cu $2p_{1/2}$. In addition, there are two satellite peaks ("Sat.") at 941.6 and 961.5 eV, which confirm the existence of Cu 2p [18]. As shown in Fig. 5d, the high-resolution Mo 3d spectrum shows that Mo $3d_{5/2}$ and Mo $3d_{3/2}$ are located at the two main peaks of 232.5 and 235.6 eV, confirming the existence of the Mo^{6+} oxidation state [19]. In the O 1 s high-resolution XPS spectra of Fig. 5e, there are two strong peaks O 1 and O 2 located at 529.8 and 531.3 eV, respectively, which are characteristics of metal oxygen bonds and defective oxygen [20]. The results of spectral analysis show the Co^{2+},Co^{3+},Cu^{2+},Mo^{6+},and O^{2-} of components contained in the $CoMoO_4$@$CuCo_2O_4$ composites.

As shown in Fig. 6a, the CV curve of the $CoMoO_4$@$CuCo_2O_4$ electrode is obtained at a scan rate of 10 mV s^{-1}. The scanning curves of the $CoMoO_4$ and $CuCo_2O_4$ electrodes are also provided for comparison. Some obvious redox peaks between the potential of − 0.2 and 0.6 V are observed on the CV curves of the $CoMoO_4$@$CuCo_2O_4$ electrode, indicating that the pseudocapacitance of the electrode material is very intense and the effect of Ni foam on the capacitance of the electrode can be ignored. The CV pattern of the $CoMoO_4$@$CuCo_2O_4$ electrode is approximately rectangular, and its area is significantly larger than that of the $CoMoO_4$ and $CuCo_2O_4$ electrodes, indicating that the composite has better pseudocapacitance behavior, and its area capacitance is larger than that of single component electrode. Figure 6b shows the CV curves of the $CoMoO_4$@$CuCo_2O_4$ electrode at different scanning rates in the potential range of − 0.2 ~ 0.6 V. The CV curve shows that the oxidation peak and reduction peak are nearly symmetrical, which can be regarded as having better Faraday pseudocapacitance characteristics. The polarization effect of electrode leads to the shift of redox peak, and these redox peaks are mainly caused by ion transfer during charging and discharging. With the increase of scanning rate, the redox peak changes greatly, and the shape is no longer symmetrical, which may be caused by the increase of internal diffusion resistance in the active material. The GCD test results of the three electrodes are shown in Fig. 6c; the specific capacitance can be calculated by Eq. (1); the GCD curves of three kinds of materials $CoMoO_4$, $CuCo_2O_4$, and $CoMoO_4$@$CuCo_2O_4$ are obtained in a potential window of 0 ~ 0.45 V; and the specific capacitance corresponds to 533, 698, and 2627 F g^{-1} at a current density of 2 A g^{-1}, respectively. In addition,

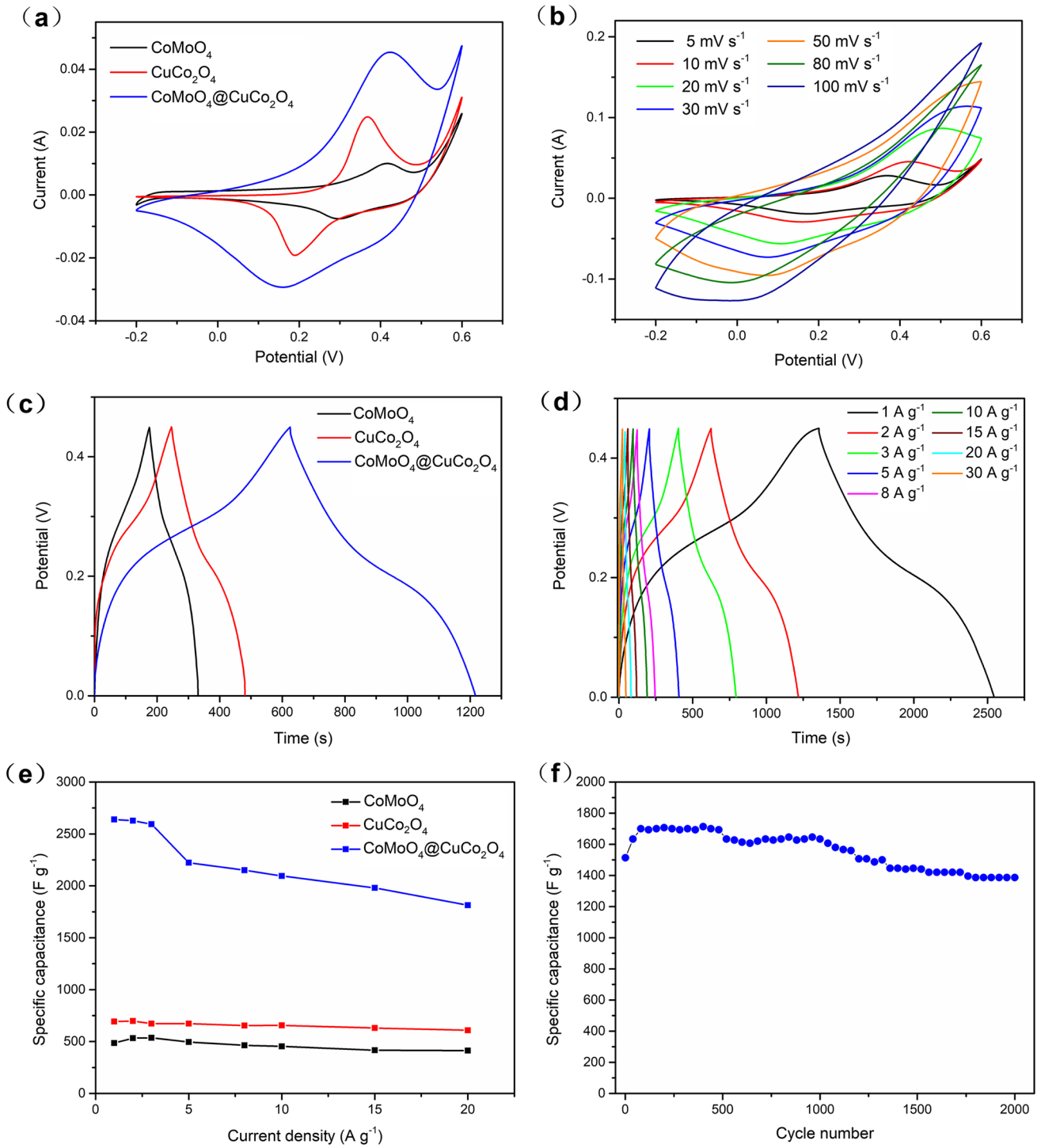

Fig. 6 **a** CV curves of $CoMoO_4$, $CuCo_2O_4$, and $CoMoO_4@CuCo_2O_4$ electrodes at 10 mV s^{-1}; **b** CV curves of the $CoMoO_4@CuCo_2O_4$ electrode conducted at various scan rates from 5 to 100 mV s^{-1}; **c** GCD curves of three products at 2 A g^{-1}; **d** GCD curves of the $CoMoO_4@CuCo_2O_4$ electrode at various current densities from 1 to 30 A g^{-1}; **e** specific capacities of $CoMoO_4$, $CuCo_2O_4$, and $CoMoO_4@CuCo_2O_4$ electrodes obtained at different current densities; **f** cycling performance of $CoMoO_4@CuCo_2O_4$ electrode for 2000 cycles

the specific capacitance of the $CoMoO_4@CuCo_2O_4$ electrode is much greater than the single $CoMoO_4$ and $CuCo_2O_4$ electrodes, representing remarkable energy storage capacity and outstanding pseudocapacitance characteristics. The specific capacitance of the $CoMoO_4@CuCo_2O_4$ electrode is greatly increased, which benefits from the synergism of

the $CoMoO_4$ microspheres and $CuCo_2O_4$ nanowires. The high conductivity of the $CoMoO_4$ microspheres and the increase of the contact area between electrode and electrolyte by the $CuCo_2O_4$ nanowires increase the electron migration rate. Therefore, the capacitance performance of the electrode is significantly improved. According to Fig. 6d, under the potential window of 0 ~ 0.45 V at current densities of 1, 2, 3, 5, 8, 10, 15, and 20 A g^{-1}, the specific capacitances of the $CoMoO_4$@$CuCo_2O_4$ electrode calculated from the discharge curve are 2639, 2627, 2593, 2222, 2151, 2095, 1980, and 1813 F g^{-1}, respectively. All the curves are approximate to symmetrical curves, indicating brilliant charge–discharge and electrochemical performance. Even at the current densities up to 30 A g^{-1}, the $CoMoO_4$@$CuCo_2O_4$ electrode still provides a high specific capacitance of 1513 F g^{-1}, which indicates that it has a superior energy storage capacity. The comparison of electrochemical performance of the $CoMoO_4$@$CuCo_2O_4$ electrode which are compared with various similar electrode materials as supercapacitor is shown in Table 1, and the electrochemical properties of the $CoMoO_4$@$CuCo_2O_4$ electrode can be better evaluated. The $CoMoO_4$@$CuCo_2O_4$ electrode exhibits an outstanding specific capacitance, which benefits from the synergistic effect of the $CoMoO_4$ microspheres and $CuCo_2O_4$ nanowires to improve the electron migration rate and significantly improve the specific capacitance of the electrode. As a result of the unique core shell structure of the hybrids, it greatly increases the specific surface area of the electrode and makes the active material fully contact with the electrolyte, which leads to the rapid increase of the electrochemical reaction rate and shows the excellent performance of electrochemical capacitors. As shown in Fig. 6e, with the increase of current density, the specific capacitance of the three electrodes gradually decreases at the same time. The specific capacitance of the $CoMoO_4$@$CuCo_2O_4$ electrode is still much greater than that of the single material electrode of $CoMoO_4$ and $CuCo_2O_4$ at the current density of 20 A g^{-1}, which finally achieved 57.3% capacity retention. Compared with the single $CoMoO_4$ and $CuCo_2O_4$ material electrodes, the $CoMoO_4$@$CuCo_2O_4$ electrode has a significant specific capacitance, which shows outstanding specific capacitance performance. The $CoMoO_4$@$CuCo_2O_4$ electrode still has excellent cycle stability at a current density of 30 A g^{-1}, and maintains 91.6% initial specific capacitance after 2000 cycles in Fig. 6f. In the initial cycle of cyclic charge and discharge, the composite material on the electrode surface is activated, and more active substances participate in the reaction, resulting in an increase in specific capacitance. During subsequent cycles, parts of the composite material on the electrode surface fall off, resulting in a decrease in the specific capacitance of the electrode. Its high specific capacitance is attributed to the unique urchin-like structure of $CoMoO_4$@$CuCo_2O_4$ composites. Its mechanism can be understood as the $CuCo_2O_4$ nanowires increase the conductivity of the $CoMoO_4$ microspheres and increase the contact area between the active material and electrolyte, so it is necessary to improve the conductivity of the $CoMoO_4$ microspheres; the $CoMoO_4$@$CuCo_2O_4$ electrode has the highest utilization rate in electrochemical reaction. In addition, the unique urchin-like structure plays a significant role in shortening the diffusion path of electrons, ions, and electrolytes, and thus effectively promoting the rapid migration of electrolyte ions during the charge–discharge process. The unique urchin-like structure can improve the structural strength of the active material, thus improving the stability of the electrode active material and greatly promoting the transport of electrolyte ions.

In the experiment, EIS test was used to further analyze the charge transport properties on the surface of supercapacitor materials. As shown in Fig. 7, the Nyquist curves of the $CoMoO_4$, $CuCo_2O_4$, and $CoMoO_4$@$CuCo_2O_4$ electrodes are similar in the frequency range of 0.01 Hz to 100 kHz. The internal resistance of the electrode is the value of the point where the high-frequency component intersects the real axis. The illustration in Fig. 7 is the equivalent circuit fitting diagram. The semicircle in the high-frequency region corresponds to the charge–discharge resistance (Rct) caused by Faraday reaction and the double-layer capacitance (Cdl) on the surface, indicating the ion diffusion resistance at the interface between the electrode and the electrolyte; the linear low-frequency component corresponds to Warburg impedance (Zw), which indicates the diffusion resistance

Table 1 Comparison of electrochemical performances of the $CoMoO_4$@$CuCo_2O_4$ electrode with previous reports

Electrode materials	Electrolyte	Specific capacitance (F g^{-1})	Current density (A g^{-1})	Capacitance retention (%)	Cycles	Reference
$CoMoO_4$	1 M KOH	1234	1	96.9	5000	[10]
$CuCo_2O_4$	6 M KOH	1131	1	79.7	5000	[11]
$NiCo_2O_4$/$CoMoO_4$	2 M KOH	1730	1	76.2	1000	[13]
$CuCo_2O_4$/$MnCo_2O_4$	2 M KOH	1434	0.5	81.4	5000	[21]
$CuCo_2O_4$@MnO_2	2 M KOH	850	1	94.2	3000	[22]
$CoMoO_4$@$CuCo_2O_4$	1 M KOH	2639	1	91.6	2000	This work

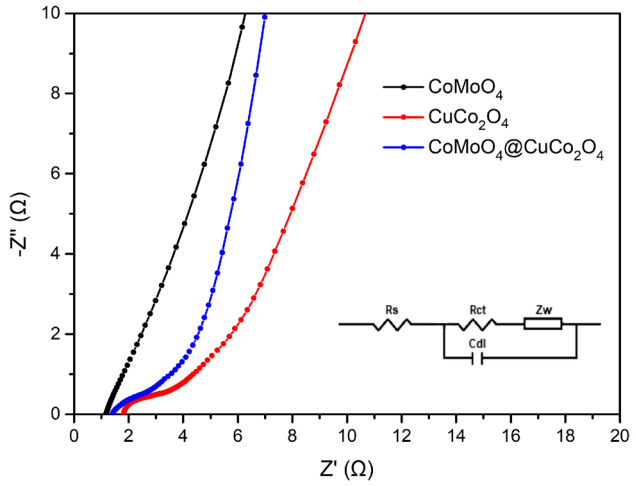

Fig. 7 EIS plots of $CoMoO_4$, $CuCo_2O_4$, and $CoMoO_4@CuCo_2O_4$ electrodes

of electrolyte. It can be seen from Fig. 7 that in the high-frequency region, the curve of the $CoMoO_4@CuCo_2O_4$ electrode is semicircle with small diameter, which indicates that the electrolyte has high conductivity and low internal resistance. The slope below the low-frequency region represents the ion diffusion resistance of the electrode/electrolyte interface. Figure 7 shows the low diffusion resistance of the electrolyte in the $CoMoO_4@CuCo_2O_4$ electrode, which leads to the increase of diffusion speed. Since the surface of the $CoMoO_4@CuCo_2O_4$ electrode is rich in active substances, electrons can be transferred quickly in the process of charge and discharge, which shortens the transmission distance between electrons and ions, thus reducing the impedance of the electrode. The unique core shell structure increases the specific surface area of the electrode, improves the cycling stability of the electrode, and promotes the redox reaction, leading to a significant improvement in capacitance performance.

For further verification practicability application value of the $CoMoO_4@CuCo_2O_4$ electrode used for the purpose of SCs, the $CoMoO_4@CuCo_2O_4$//AC ASC device was formed by using the $CoMoO_4@CuCo_2O_4$ electrode as positive electrode and AC on Ni foam as negative electrode. Figure 8a exhibits the CV test of the $CoMoO_4@CuCo_2O_4$//AC ASC device at 20 mV s^{-1} scan rate in a voltage window from 0.6 to 1.8 V. With the increase of the voltage window, the area of the CV curve increases gradually. When the voltage window reaches 1.6 V, it shows excellent electrochemical activity and pseudocapacitance characteristics, which is the best working window potential of the ASC device. Figure 8b shows the CV test image of the ASC device at scanning rate of 10 ~ 100 mV s^{-1} at 0 ~ 1.6 V voltage window. With the increase of scanning rate, the CV curves have no obvious disproportion, and the curve keeps a symmetrical shape, which indicates that the ASC device has excellent reversibility. As shown in Fig. 8c, the GCD curves of the ASC device under different current densities can fully prove that the ASC device has pseudocapacitance characteristics. With the increase of current density, the discharge time of the ASC device decreases in turn, which indicates that there may be non-reversible redox reaction on the electrode surface, and some active substances have not been able to participate in the electrochemical reaction. At the same time, there is no symmetry in the shape of the GCD curve, which indicates that there are some irreversible redox reactions in the process of charge and discharge. In Fig. 8d, according to the specific capacitance calculation formula, it can be concluded that the specific capacitances of the $CoMoO_4@CuCo_2O_4$// AC ASC device are 144.3, 103.4, 100.1, and 55.6 F g^{-1} at the current densities of 1, 2, 3, 4, and 5 A g^{-1}, respectively. The ASC device can obtain a high specific capacitance of 52 F g^{-1} at a current density of 8 A g^{-1}, which shows the remarkable energy storage capacity of the ASC device. In the practical application of the ASC device, cycle stability is a key performance parameter in practical application. The ASC device has completed 2000-cycle tests at a current density of 5 A g^{-1} and finally maintains 87.9% of the initial specific capacitance which demonstrates distinguished cycle stability in Fig. 8e. According to the known specific capacitance, the energy density and power density of the supercapacitor are calculated by Eqs. (2) and (3). In Fig. 8f, the energy density of the ASC is 51.2 W h kg^{-1}, when the power density is 800.3 W kg^{-1}, which maintains the energy density of 16.89 W h kg^{-1} at the power density of 6400 W kg^{-1}. It is fully demonstrated by the line diagram in Fig. 8f that the ASC device can provide high energy density and power density, and provide electrical energy for electronic devices, which has excellent application prospect and application value. The $CoMoO_4@CuCo_2O_4$//AC ACS device is a high-performance energy storage device which compares with electrodes of similar materials; the energy density and power density of the ACS device are significantly improved, providing a new method for synthesizing high-efficiency electrode structures.

Conclusion

In summary, the $CoMoO_4@CuCo_2O_4$ composites were successfully synthesized on Ni foam by hydrothermal method and annealing method. It has eminent electrochemical activity and pseudocapacitance characteristics. The synthesized $CoMoO_4@CuCo_2O_4$ electrode has a specific capacitance of 2639 F g^{-1} at a current density of 1 A g^{-1} and 1513 F g^{-1} at a current density of 30 A g^{-1}, which maintains 91.6% initial specific capacitance after 2000 cycles as well. The distinguished stability is attributed to the core shell structure

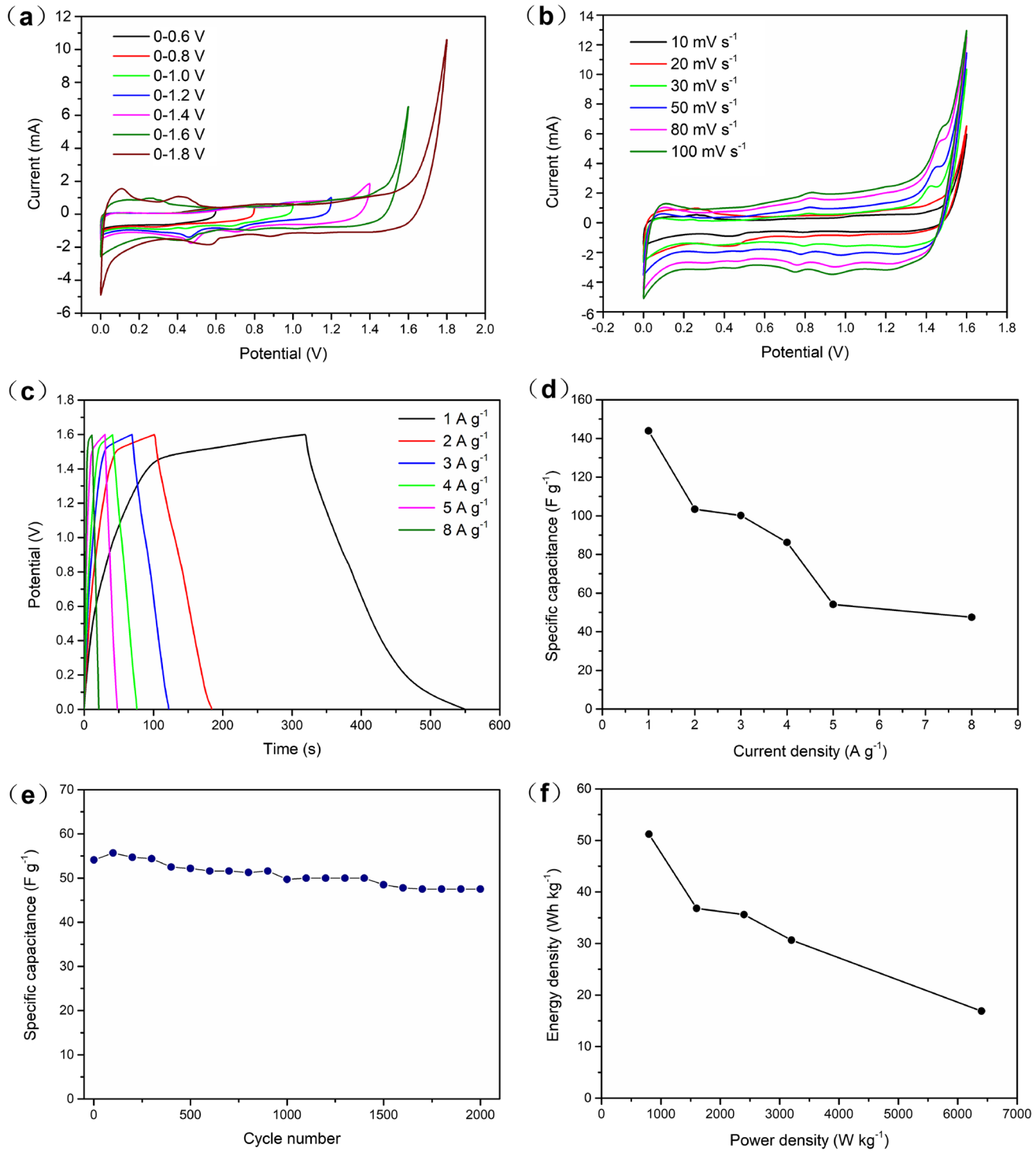

Fig. 8 **a** CV curves of the $CoMoO_4$@$CuCo_2O_4$//AC ASC at dissimilar voltage ranges with a scan rate of 20 mV s^{-1}; **b** CV curves of the $CoMoO_4$@$CuCo_2O_4$//AC ASC with dissimilar scan rates at a voltage window of 0 ~ 1.6 V; **c** GCD curves of the $CoMoO_4$@$CuCo_2O_4$//AC ASC device at dissimilar current densities; **d** the specific capacitance of the $CoMoO_4$@$CuCo_2O_4$//AC ASC device corresponds to dissimilar current densities; **e** cycling performance of the $CoMoO_4$@$CuCo_2O_4$//AC ASC device for 2000 cycles; **f** the Ragone plots relating power density to energy density of $CoMoO_4$@$CuCo_2O_4$//AC ASC device

and the synergistic effect of the two materials, which makes the specific capacitance better than single component electrode. Furthermore, the ASC device based on the $CoMoO_4$@$CuCo_2O_4$ electrode as positive electrode and AC on Ni foam as negative electrode obtains a high energy density of 51.2 W h kg^{-1} at a power density of 800.3 W kg^{-1}, and which maintains a energy density of 16.89 W h kg^{-1} at a power density of 6400 W kg^{-1}. The ASC device demonstrated excellent cycling life after 2000 cycles and maintained 87.9% of the initial specific capacitance. These experimental results show that the $CoMoO_4$@$CuCo_2O_4$ electrode is a high-performance electrode material with high capacity and excellent stability, which is a potential material for the development of SCs. With the development of portable electronic devices, the preparation materials of supercapacitors are becoming more and more diversified, and the preparation of flexible and foldable supercapacitors has become the focus of the following research.

Acknowledgements We would like to thank the Engineering Research Center of Agricultural Multi-Dimensional Sensor Information Perception, Heilongjiang Province, and Heilongjiang Provincial Key Laboratory of Micro-Nano Sensor Component. This work was jointly supported by the Fundamental Research Funds in Heilongjiang Provincial Universities (Nos. 135109244, 135309115, 135309211, and 135409104), Heilongjiang Science Foundation Project (JQ2019F003 and ZD2019F004).

References

1. Liu Y, Xiang C, Chu H, Qiu S, McLeod J, She Z, Xu F, Sun L, Zou Y (2020) Binary Co-Ni oxide nanoparticle-loaded hierarchical graphitic porous carbon for high-performance supercapacitors. J Mater Sci Technol 37(02):135–142
2. Liu A, Tang J (2020) Construction of polypyrrole-wrapped hierarchical $CoMoO_4$ nanotubes as a high-performance electrode for supercapacitors. Ceram Int 46(8):10893–10902
3. Zhang P, He H, Li Q (2020) Ni-Co-S nanosheets supported by $CuCo_2O_4$ nanowires for ultra-high capacitance hybrid supercapacitor electrode. Int J Hydrogen Energy 45(7):4784–4792
4. Zheng Y, Li Z, Xu J, Wang T, Liu X, Duan X, Ma Y, Zhou Y, Pei C (2016) Multi-channeled hierarchical porous carbon incorporated Co_3O_4 nanopillar arrays as 3D binder-free electrode for high performance supercapacitors. Nano Energy 20:94–107
5. Li Y, Wang X, Yang Q, Javed MS, Liu Q, Xu W, Hu C, Wei D (2017) Ultra-fine CuO nanoparticles embedded in three-dimensional graphene network nano-structure for high-performance flexible supercapacitors. Electrochim Acta 234:63–70
6. Gueon D, Moon JH (2017) MnO_2 nanoflake-shelled carbon nanotube particles for high-performance supercapacitors. ACS Sustainable Chemistry & Engineering 5(3):2445–2453
7. Yadav AA, Hunge YM, Liu S, Kulkarni SB (2019) Ultrasound assisted growth of $NiCo_2O_4$@carbon cloth for high energy storage device application. Ultrasonics Sonochem 56:290–56296
8. Xu G, Zhang Z, Qi X, Ren X, Liu S, Chen Q, Huang Z, Zhong J (2018) Hydrothermally synthesized $FeCo_2O_4$ nanostructures: structural manipulation for high-performance all solid-state supercapacitors. Ceram Int 44(1):120–127
9. Peng S, Li L, Hao BW, Madhavi S, Xiong W (2015) Controlled growth of $NiMoO_4$ nanosheet and nanorod arrays on various conductive substrates as advanced electrodes for asymmetric supercapacitors. Adv Energy Mater 5(2):1–7
10. Long H, Liu T, Zeng W, Yang Y, Zhao S (2018) $CoMoO_4$ nanosheets assembled 3D-frameworks for high-performance energy storage. Ceram Int 44(2):2446–2452
11. Liu S, Hui K, Hui KN (2016) Flower-like copper cobaltite nanosheets on graphite paper as high-performance supercapacitor electrodes and enzymeless glucose sensors. ACS Appl Mater Interfaces 8(5):3258–3267
12. Feng Y, Liu L, Liang J, Yao W, Tian B, Jiang C, Wu W (2019) $Ni(OH)_2$/$NiMoO_4$ nanoplates for large-scale fully-printed flexible solid-state supercapacitors. Elsevier 433(126676):1 126676.8
13. Wu Y, Guo W, Lian X, Tian Y, Wang W, Li J, Wang S (2019) Self-assembled three-dimensional hierarchical $CoMoO_4$ nanosheets on $NiCo_2O_4$ for high-performance supercapacitor. J Alloys Compound 793(15):418–793424
14. Nti F, Anang DA, Han JI (2018) Facilely synthesized $NiMoO_4$/$CoMoO_4$ nanorods as electrode material for high performance supercapacitor. Alloy Compd 742:342–350
15. Chen H, Wang J, Han X, Liao F, Zhang Y, Han X, Xu C (2019) Simple growth of mesoporous zinc cobaltite urchin-like microstructures towards high-performance electrochemical capacitors. Ceram Int 45(3):4059–4066
16. Wu H, Sun W, Shen J, Rooney DW, Wang Z, Sun K (2018) Role of flower-like ultrathin Co_3O_4 nanosheets in water splitting and non-aqueous Li-O_2 batteries. Nanoscale 10(21):10221–10231
17. Liu Y, Lu Q, Huang Z, Sun S, Yu B, Evariste U, Jiang G, Yao J (2018) Electrodeposition of Ni-Co-S nanosheet arrays on N-doped porous carbon nanofibers for flexible asymmetric supercapacitors. J Alloy Compd 762:301–311
18. Shanmugavani A, Selvan RK (2016) Improved electrochemical performances of $CuCo_2O_4$/CuO nanocomposites for asymmetric supercapacitors. Electrochim Acta 188:852–862
19. Cao Y, An L, Liao L, Liu X, Ji T, Zou R, Yang J, Qin Z, Hu J (2016) Hierarchical core/shell structures of ZnO nanorod@$CoMoO_4$ nanoplates used as a high-performance electrode for supercapacitors. RSC Adv 6:3020–3024
20. Cui C, Xu J, Wang L, Guo D, Mao M, Ma J, Wang T (2016) Growth of $NiCo_2O_4$@$MnMoO_4$ nanocolumn arrays with superior pseudocapacitor properties. ACS Appl Mater Interfaces 8(13):8568–8575
21. Liu S, Hui KS, Hui KN, Yun JM, Kim KH (2016) Vertically stacked bilayer $CuCo_2O_4$/$MnCo_2O_4$ heterostructures on functionalized graphite paper for high-performance electrochemical capacitors. Journal of Materials Chemistry A 4:8061–8071
22. Min K, Xiao Y, Fan D, Yu X (2015) Tunable design of layered $CuCo_2O_4$ nanosheets@MnO_2 nanoflakes core–shell arrays on Ni foam for high-performance supercapacitors. Journal of Materials Chemistry A 3(43):21528–21536